Variability of Tropical Diurnal Sea Surface Temperature*

CAROL ANNE CLAYSON AND DERRICK WEITLICH

Department of Meteorology, The Florida State University, Tallahassee, Florida

(Manuscript received 18 August 2005, in final form 30 May 2006)

ABSTRACT

A dataset consisting of daily diurnal warming values from 1996 through 2000 covering the global Tropics (30°N through 30°S) at 0.25° × 0.25° resolution has been created using a parameterization for the diurnal warming developed previously. The inputs to the parameterization are the peak shortwave solar radiation [determined from International Satellite Cloud Climatology Project (ISCCP) data] and daily averaged wind speed [determined from Special Sensor Microwave Imager (SSM/I) data]. Comparisons with Tropical Ocean Global Atmosphere (TOGA) Tropical Atmosphere Ocean (TAO) and Pilot Research Moored Array in the Tropical Atlantic (PIRATA) buoys show that the biases are small (mean bias is 0.0012°C; the standard deviation and correlation are 0.26°C and 0.74) and show no discernable geographic bias.

The 5-yr average shows that throughout most regions the values are small, with higher values (approaching 1°C) in the northern Indian Ocean, the western equatorial Pacific, the equatorial eastern Pacific, and several coastal regions. An EOF analysis of the variability indicates that seasonal variability is the most dominant form for each of the basins; in the Atlantic and Pacific basins it is north–south following the solar cycle. In the Indian Ocean the seasonal cycle is dominated by monsoonal variability; both the northern and southern portions of the basin have above-mean or below-mean values at the same times. Seasonal shortwave variability is responsible for the second mode in the Indian Ocean. East–west dipole weight structures appear in the spatial patterns for mode 2 in the Pacific and mode 3 for the Atlantic and Indian Oceans. These modes also display seasonally varying characteristics, with late 1997 and early 1998 being somewhat anomalous in the Pacific and Indian Oceans.

1. Introduction

Convection in the tropical oceans, particularly the western tropical Pacific and eastern Indian Ocean, occurs on many scales. Smaller clouds and cloud clusters are affected by the diurnal cycle, as are larger mesoscale clusters (e.g., Mapes and Houze 1995). Diurnal variability in the Tropics, due to the large variation in day/night surface solar radiation, affects both sea surface temperature (SST) and convective variability. Sea surface temperature variability in the tropical oceans is fundamentally coupled to variations in convection and cloud–radiation feedbacks. Numerous studies have documented the importance of several modes of SST variability in the Pacific, such as the El Niño–Southern Oscillation (ENSO) cycle and its relationship to convection both locally and extratropically (e.g., Webster and Lukas 1992; McPhaden et al. 1998). Interannual SST variability in the Atlantic, associated with ENSO (e.g., Chang et al. 1997), the so-called Atlantic dipole (e.g., Huang and Shukla 1997), and equatorial warm events (Chang et al. 1997) are coupled with changes in the location of the intertropical convergence zone. At all of these time scales, SSTs can affect rainfall and convection in the Indian Ocean region (Perigaud et al. 2003).

It is becoming clear that diurnal variability of the upper ocean and surface temperature can affect longer time-scale variability of both the ocean and the atmosphere. Shinoda (2005) emphasized the role of diurnal warming and entrainment cooling in modulating intraseasonal sea surface temperature variability in the western Pacific warm pool region, with positive feedbacks elevating sea surface temperatures throughout the suppressed phase of intraseasonal oscillations.

* Geophysical Fluid Dynamics Institute Contribution Number 448.

Corresponding author address: Carol Anne Clayson, Department of Meteorology, and Geophysical Fluid Dynamics Institute, 404 Love Building, The Florida State University. Tallahassee, FL 32306.
E-mail: clayson@met.fsu.edu

DOI: 10.1175/JCLI3999.1

Simulations of the ENSO cycle by Solomon and Jin (2005) indicated that inclusion of the diurnal mixing within a coupled model demonstrably changed interannual variability. Sui et al. (1997) highlighted the effects of diurnal warming on the upper ocean and the longer time scale. Resolving the diurnal change in skin SST has also been examined with increasing interest to view possible feedbacks that it has on the atmosphere (Clayson and Chen 2002).

Accurate determination of the diurnal warming is necessary to understand the importance of the diurnal cycle in SST to longer-scale variability in the ocean and atmosphere. The diurnal warming can be on the order of 3°C or more in the Tropics under calm and clear conditions (Fairall et al. 1996; Soloviev and Lukas 1997). Early studies of the diurnal sea surface temperature focused on in situ observations, including observations in the Atlantic near Bermuda (Stommel 1969), near the coast of northwest Africa (Halpern and Reed 1976), and the west coast of California (Price et al. 1986). These studies were necessarily limited in space and time. Satellite observations offered the advantages of increased spatial and temporal coverage; the use of day/night passes allowed Deschamps and Frouin (1984), in the Mediterranean Sea, and Stramma et al. (1986), near the Long Term Upper Ocean Study (LOTUS) mooring in the Atlantic, to deduce diurnal SST warming, with maximum values of 3.5°C.

These studies noted the concurrence of higher diurnal warming with increased solar radiation and decreased winds. One of the original parameterizations that was developed to relate the diurnal sea surface temperature variability to the surface fluxes was by Price et al. (1986), who used surface heat flux and wind stress as inputs. Using data from the Tropical Ocean Global Atmosphere (TOGA) Coupled Ocean–Atmosphere Response Experiment (COARE) program in the tropical western Pacific, an equation was developed to compute the amplitude of the diurnal change or, in other words, the diurnal warming in skin SST, referred to here as dSST (Webster et al. 1996). The dSST is defined as the difference between the peak daytime value and the nighttime SST minimum (near daybreak: see Fig. 1). They found that diurnal forcing from atmospheric variables plays a large role in determining the magnitude of the diurnal warming seen in the skin SST. The equation created uses values of the magnitude of the peak solar insolation, the cumulative amount of daily precipitation, and average daily wind speed to compute the dSST. The effect of varying ocean stratification on the diurnal SST, or in other words the extent to which the parameterization can adequately model the dSST, was evaluated in the tropical oceans by Clayson and Weitlich (2005). More recently Kawai and Kawamura (2002) and Gentemann et al. (2003) have followed similar approaches.

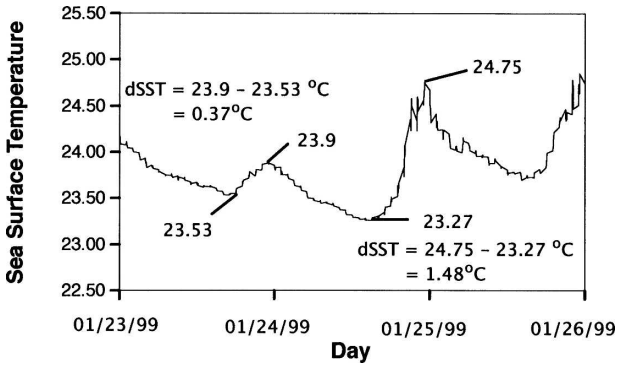

FIG. 1. Several days of SST observations from a TAO buoy, along with indications of the predawn and maximum SST and resulting dSST value for two of the days.

Several studies have examined the diurnal warming of SSTs in certain regions around the world, mostly with in situ data. Recently a global climatology study of diurnal warming using satellite-derived SST was conducted (Stuart-Menteth et al. 2003). They examined the diurnal warming of SSTs directly from Advanced Very High Resolution Radiometer (AVHRR) SST values. Their findings showed that large regions in both the midlatitudes and Tropics showed frequent diurnal warming with a strong seasonal pattern influenced by wind and solar insolation variability. Cloud contamination in the Tropics led to a great deal of missing data and therefore could not reveal complete information of diurnal warming in this region. Gentemann et al. (2003) used Tropical Rainfall Measuring Mission (TRMM) Microwave Imager (TMI) data to examine diurnal warming in the Tropics, although data pixels under clouds were not used, leading to incomplete coverage.

In this study we use a diurnal-warming sea surface temperature dataset created using the Clayson and Curry (1996) methodology with some adaptations for the period of 1996–2000 to explore the variation of the diurnal warming in the tropical ocean basins. This diurnal warming dataset is described below, some comparisons with buoy data are performed, and mean characteristics of the data are shown.

This dataset calculates the diurnal warming at each location in the global tropical oceans every day. This differs from the available satellite retrievals, for instance from TMI, in that each instrument would need to pass each location in the Tropics twice a day at the appropriate times (predawn and peak value, as shown in Fig. 1). The frequency with which the TMI passes any given location in the Atlantic in one 15-day period is

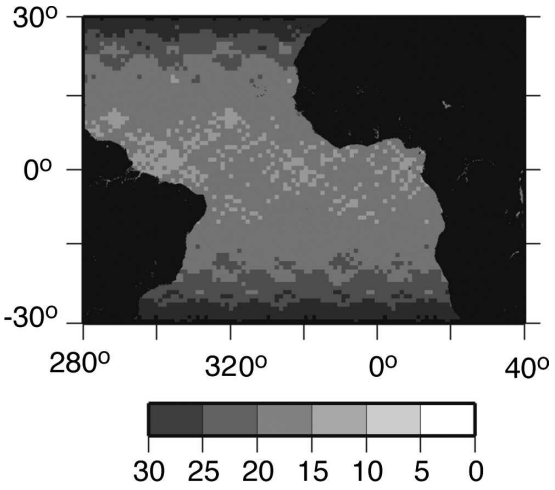

FIG. 2. Number of times within a 15-day period the TRMM satellite passes a given 0.5° × 0.5° box in the tropical Atlantic. Only at those points with at least 30 observations would there be a possibility of observing the dSST value at this spatial scale.

shown in Fig. 2 for a 0.5° × 0.5° box; for instance, at no location in the tropical oceans over a 6-month period in 1999 is there a measurement on a given day of both the predawn value and the peak SST. If, however, the size of the box were expanded to say 2.5° × 2.5°, roughly 10% of the global Tropics would, on any given day, have diurnal warming coverage. However, a much larger box introduces the possibility for significant error, as the predawn measurement could have been taken from a region more than 200 km away from the maximum SST measurement, and the differences in temperature in regions of high horizontal SST variability would then reflect that horizontal SST variability rather than the warming at a single location. In addition, given the 23-day (equator) to 46-day (at TRMM's highest latitude) cycle in local viewing times (e.g., Imaoka and Spencer 2000), the temporal resolution of the diurnal warming dataset is necessarily reduced from daily to near monthly.

2. Data, methodology, and error characteristics

The method of Clayson and Curry (1996) has been applied to data obtained by the International Satellite Cloud Climatology Project (ISCCP) and Special Sensor Microwave Imager (SSM/I) data to produce a daily diurnal variation in SST database for the global Tropics during the years 1996–2000. Since the equation from Webster et al. was implemented for this task, a database of dSST values for the same period was created. These diurnal warming values represent an alternative way of examining the diurnal SST variability over many spatial and temporal scales. This initial dataset included the use of shortwave radiation (SWR) and wind speed. The SWR was obtained from the ISCCP and the wind speed was retrieved from SSM/I data. For comparison purposes between the satellite-derived and observed diurnal warming values, in situ data was obtained from the Tropical Atmosphere Ocean/Triangle TransOcean Buoy Network (TAO/TRITON) and Pilot Research Moored Array in the Tropical Atlantic (PIRATA) buoys. The data and methodology are described here, as are comparisons and error characteristics of the diurnal warming dataset.

a. Data description

1) ISCCP SWR AND SST

Total SWR was determined for this project from the ISCCP-F DX dataset (Zhang et al. 2004). This dataset uses radiances from NOAA Polar Orbiting Environmental Satellites (POES), Geostationary Operational Environmental Satellites (GOES), Geostationary Meteorological Satellites (GMS), and Meteosat geostationary satellites to determine cloud properties. The shortwave radiances are converted to surface flux values through a spectral radiative transfer model with ISCCP-derived cloud properties as input parameters, following the methodology of Zhang et al. (1995). The effects of such features as aerosols, water vapor, and other atmospheric gaseous absorbers, as well as cloud microphysics, are included in the radiative transfer model. Comparisons with such datasets as the Baseline Surface Radiation Network have shown monthly mean biases on the order of 2.0 W m^{-2}, rms differences of 18.5 W m^{-2}, and correlation coefficients of 0.98 for downwelling surface shortwave radiation (Zhang et al. 2004).

ISCCP data were available for every 3 h beginning at 0000 UTC. The data were used in the global tropical latitudes ranging from 30°N to 30°S and have a spatial resolution of 0.5° latitude × 0.5° longitude. For each latitude and longitude pixel the maximum SWR value for each day (local time considered) was found during the period from 1 January 1996 to 31 December 2000. In some instances data was not available for calculating a peak SWR; the year with the most missing SWR data was 1996 (with 7%); 2000 had the least (0.25%). Spatial interpolation of SWR peaks was performed to eliminate the missing data. Accuracies of the peak SWR used for the dSST calculations are shown below.

The SST data used for predawn temperature values were the clear-sky composite temperatures, at a spatial resolution of 0.25° latitude × 0.25° longitude. Using the methodology of Clayson and Curry (1996), temporal

interpolation was used to fill in missing data (generally due to cloudy conditions) for these predawn values. These predawn SSTs were then combined with the diurnal cycle as calculated below to form a complete global tropical SST map at 0.25° latitude and longitude every 3 h for the years 1996 through 2000. In comparison with ship-measured skin temperatures during the TOGA COARE Intensive Observations Phase this method showed mean bias of 0.08°C, rms error of 0.34°C and a correlation coefficient of 0.75. In this research, the calculated SSTs are used only to show mean conditions at various times; in all other instances, only the diurnal variability is shown, which does not require the use of the ISCCP SST; comparisons below aimed at understanding errors in the diurnal warming dataset thus focus only on the computed dSST values. The full SST dataset can be found online (at http://seaflux.gfdi.fsu.edu).

2) SSM/I WIND SPEEDS

Wind speeds were calculated from brightness temperatures measured from the Special Sensor Microwave Imager radiometers onboard the Defense Meteorological Satellite Program polar orbiting satellites. As part of the NASA Pathfinder Program, SSM/I data are used to find ocean wind speed at 10 m, water vapor, cloud water, and rain rate. SSM/I version-5 data, downloaded from ftp.ssmi.com, were used for this study. These data use an improvement to the Wentz algorithm (Wentz 1997) to convert radiances to the atmospheric variables previously mentioned. The previous algorithm showed collocated satellite/buoy mean biases of 0.4 m s^{-1}, with slightly higher biases at wind speeds less than 5 m s^{-1}, with standard deviations of less than 1.4 m s^{-1} (Mears et al. 2001). Accuracies of the daily wind speeds used for the dSST calculations and the impact of the errors are shown below. The data have a spatial resolution of 0.5° latitude × 0.5° longitude. For each pixel, the available SSM/I wind speed data that were measured during different times of the day were averaged to obtain the 10-m daily-averaged wind speed. If no daily-averaged wind speed values were found for a particular location due to spaces between satellite measurement passes, temporal interpolation was performed using the days immediately preceding and following the missing data.

3) TAO/TRITON AND PIRATA BUOY DATA

The TAO array, now referred to as the TAO/TRITON array, consists of on average 70 buoys that lie in the tropical Pacific between latitudes 8°N and 8°S and a longitude range between 95°W and 137°E (e.g., McPhaden et al. 1998). The PIRATA program started in late 1997 and consists of 12 moored buoys in the tropical Atlantic. These buoys have a range within 15°N and 10°S, 0° and 38°W. Like the TAO/TRITON buoys, the PIRATA array also measures key atmospheric surface variables and upper ocean characteristics (Servain et al. 1998).

High-resolution (10 min) SST data measured at 1 m were obtained from several buoys within the TAO/TRITON and PIRATA arrays (locations shown in Fig. 5) from the TAO Project Web site (http://www.pmel.noaa.gov/tao/disdel/). The buoys were chosen because they measured both downwelling SWR (measured at 3.5 m above sea level and at 2-min resolution) and wind speed (4 m above sea level at 10-min resolution). All comparisons were performed for 1999; dSST was determined for all points as in Fig. 1. To analyze differences between the dSST values derived from the satellite parameterization and the buoy measurements, maximum SWR values were found from an 18-min running mean value of shortwave radiation from the buoys for each day. Also, wind data were adjusted to wind speeds at 10 m using a log wind profile with stability considerations (Bourassa et al. 1999). This conversion required buoy values of air temperature and specific humidity, which were acquired as well. However, a few buoys had to be eliminated from the wind comparisons since they did not have one or both of these values. This wind speed was averaged over 24 h. The quoted accuracies for the wind speed, downwelling shortwave radiation, and sea surface temperature measurements are ±0.3 m s^{-1}, ±1%, and ±0.02°C (Payne et al. 2002).

b. Methodology

The amplitude of diurnal warming (dSST) is calculated from the parameterization of Clayson and Curry (1996), based on the analysis of diurnal sea surface temperature of Webster et al. (1996). This parameterization is a regression equation that uses the values of peak insolation, daily averaged wind speed, and daily averaged precipitation based on model simulations:

$$\mathrm{dSST} = f + a(\mathrm{PS}) + b(\mathrm{P}) + c\ln(U) + d(\mathrm{PS})\ln(U) + e(U), \quad (1)$$

where PS is the peak solar insolation (W m^{-2}), U is the daily averaged 10-m wind speed (m s^{-1}), and P is the daily averaged precipitation (mm h^{-1}). The coefficients in Eq. (1) are determined differently for $U > 2$ m s^{-1} and $U \leq 2$ m s^{-1} (Table 1). Clayson and Curry used this parameterization to develop a 3-hourly SST field from satellite data for comparison with data during the TOGA COARE period, and for this limited compari-

TABLE 1. Coefficient values for dSST equation [Eq. (1)] for different daily averaged wind speeds.

Coefficient	$U > 2$ m s^{-1}	$U \leq 2$ m s^{-1}
f	0.262	0.328
a	0.002 65	0.002
b	0.028	0.041
c	−0.838	0.212
d	−0.001 05	−0.000 185
e	0.158	−0.329

son it was found to have an overall bias of less than 0.05°C, with a maximum bias of 0.07°C at very high wind speeds.

This parameterization is used in this study with the ISCCP-derived peak SWR values and 10-m wind speed to determine the diurnal warming for every day in the period of 1 January 1996 through 31 December 2000 at a 0.25° × 0.25° resolution. Complete precipitation fields were not available and were set to zero. As can be seen in the Webster et al. calculations, diurnal warming dependence on precipitation is the smallest of the three inputs and is most influential under high precipitation inputs and weak winds, with the average maximum effect on dSST being roughly 0.3°C. Future work will compare the importance of including precipitation.

Once the complete fields of diurnal warming were created, average fields over various times were used to understand mean diurnal warming conditions and their differences from basin to basin. To better visualize the patterns of variability in both time and space in large datasets such as the diurnal warming dataset, empirical orthogonal function (EOF) analyses were performed. In the entire diurnal warming dataset there are 297 498 spatial values (excluding land pixels) that are measured over 1827 days. The three basins were evaluated separately, with the Atlantic Ocean EOF analyses covering the longitudes 80°W to 20°E, the Indian Ocean EOF analyses covering 30° to 120°E, and the Pacific Ocean analyses covering 120°E to 80°W; with the same latitudinal coverage (30°N to 30°S). The results of these analyses will be presented in the following sections.

c. Comparisons

A difficulty in comparing the diurnal warming as evidenced from the satellite-derived dataset and the buoy dataset is that the parameterization is derived for the skin surface temperature, and the highest buoy recorded sea surface temperature is at 1 m. A damping of the diurnal warming with depth in the water column has been noted by a number of researchers (e.g., Fairall et al. 1996; Clayson and Chen 2002); Webster et al. (1996) estimated that the differences during periods characterized by high solar insolation and calm winds between the skin and at 0.5 m were 0.3°C. Using the average SWR and wind speed during all conditions studied here, this difference was on average 0.12°C. The buoy measurements in this study could not be converted to skin temperature because the buoys did not have downwelling longwave radiation data, which is needed to do an accurate correction to skin temperatures. In addition, any changes in surface temperature due to advection between the predawn time and the peak solar radiation time could lead to uncorrectable errors in the satellite estimation.

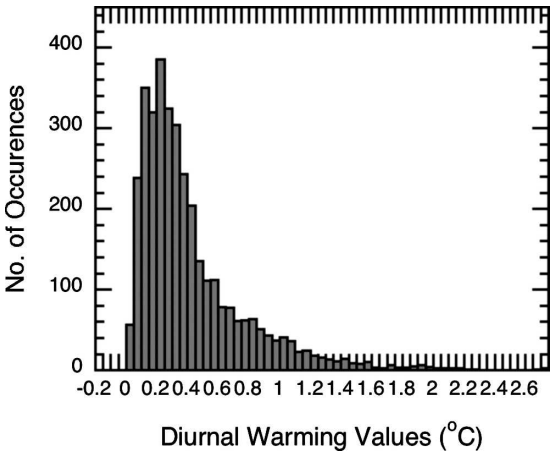

FIG. 3. Histogram of observed buoy dSST values.

A second difficulty arises in estimating the errors in the satellite values of SWR and wind speed as compared to errors in the parameterization itself. The SWR and wind speed values are roughly 50-km satellite measurements as compared to the buoy point measurements. This is especially problematic when comparing SWR. Rossow and Zhang (1995) compared the ISCCP downwelling SWR to data from the TOGA COARE pilot cruise in 1990 and found that most of the differences between the two datasets were attributable to spatial sampling issues (see also Seze and Rossow 1991). Bourassa et al. (2003) showed by comparing Quick Scatterometer (QuikSCAT) wind data to ship observations that there is substantial natural variability on spatial scales less than 25 km.

The 21 buoys provided 3517 diurnal warming values in 1999 for comparison with the calculated values. Several diurnal amplitude values greater than 2°C, though rare, did occur in the buoy dataset with a maximum of 2.70°C (Fig. 3); however there are no values greater than 1.96°C (Fig. 4) in the satellite-derived data. A possible explanation for this is discussed later. The buoy and satellite-derived observations both showed a median dSST value of 0.31°C; mean values for both

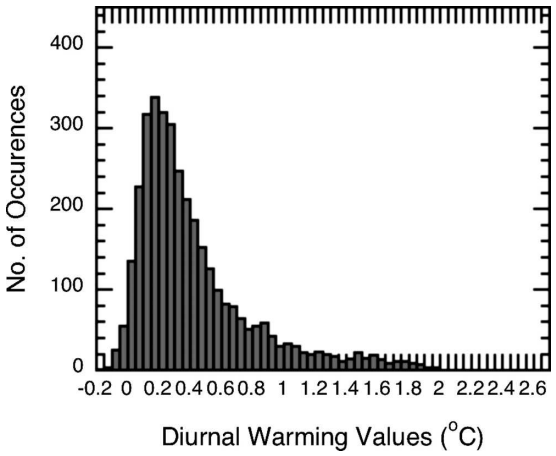

FIG. 4. Histogram of satellite-derived dSST values.

datasets were also similarwith values near 0.42°C. The average bias (observed minus satellite-derived) and correlation of the dSST comparisons for each buoy location are shown in Table 2; no regional biases are evident (as can be seen in Fig. 5). The biases range from −0.174° to 0.129°C; the mean bias is 0.0012°C with a standard deviation of 0.26°C and correlation of 0.74. Correlations at each of the buoy locations range from 0.28 to 0.83, with most correlations above 0.50. Higher correlations dominate the PIRATA buoy locations, while TAO/TRITON correlations tend to be slightly lower. The histogram for all bias values forms a roughly Gaussian curve, visible in Fig. 6.

There are several ways for errors in the satellite-derived dSST to occur. One is by errors in the input fields of SWR and wind speed, and another is through the dSST parameterization itself. Webster et al. (1996) found an overall bias in the parameterization of less than 0.05°C. An examination of the biases and correlations for the satellite SWR and wind speed values show substantially larger biases in SWR and small biases in wind speed. The satellite measurements underestimate the maximum SWR relative to the buoy with most biases over 100 W m^{-2} (a histogram of these biases for the entire dataset is shown in Fig. 7). Correlations between the two measurements are also smaller than those calculated from the dSST values, ranging from −0.05 to 0.78. The average bias for maximum SWR for the whole comparison dataset is 133.97 W m^{-2} with an overall correlation of 0.48. This is a large bias for this study due to the fact that at low wind speeds

TABLE 2. Average bias and correlation (corr) values of comparisons between the buoy and satellite-derived dSST values.

TAO/TRITON	PIRATA
Lat, lon (deg min): bias (°C), corr	Lat, lon (deg min): bias (°C), corr
0°, 110°W: −0.019, 0.60	0°, 10°W: 0.029, 0.68
0°, 125°W: 0.027, 0.51	0°, 23°W: 0.073, 0.80
0°, 165°E: −0.040, 0.59	0°, 35°W: 0.129, 0.53
2°N, 165°E: −0.019, 0.51	10°S, 10°W: −0.022, 0.83
2°S, 165°E: −0.159, 0.79	12°N, 38°W: 0.001, 0.70
2°S, 95°W: −0.174, 0.58	15°N, 38°W: −0.013, 0.73
5°N, 165°E: −0.049, 0.45	2°N, 10°W: 0.026, 0.28
5°S, 165°E: −0.070, 0.56	2°S, 10°W: 0.028, 0.59
5°S, 95°W: 0.050, 0.62	5°S, 10°W: −0.019, 0.75
8°S, 165°E: 0.050, 0.49	8°N, 38°W: 0.009, 0.55
8°S, 95°W: 0.014, 0.79	

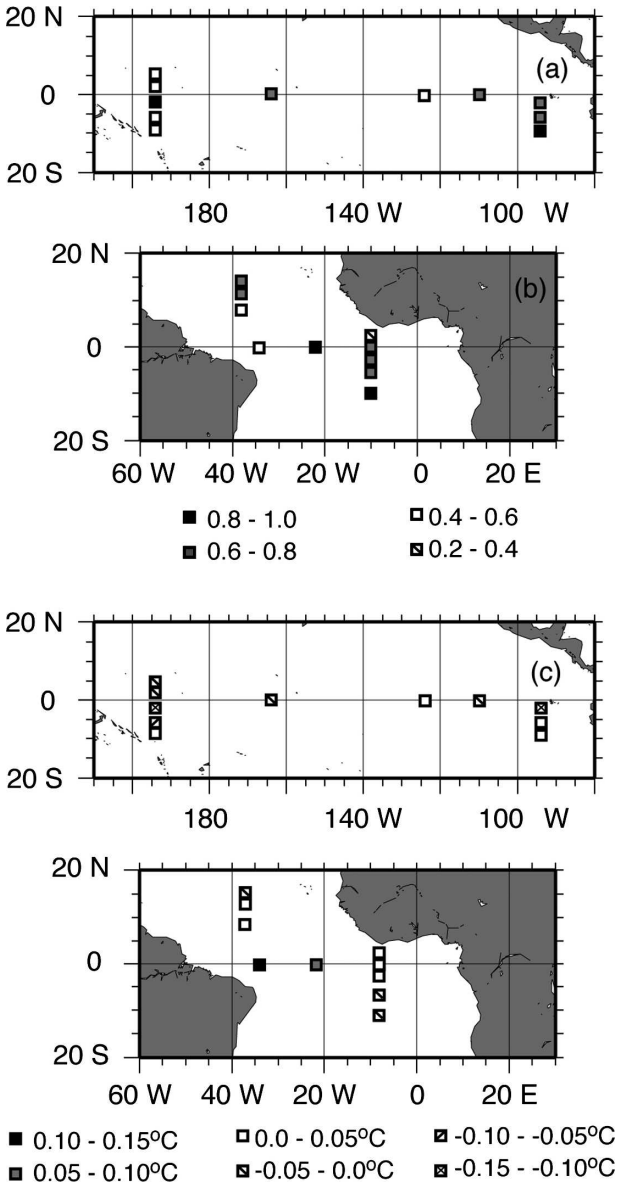

FIG. 5. (a), (c) Bias and (b), (d) correlations for the Pacific and Atlantic comparisons.

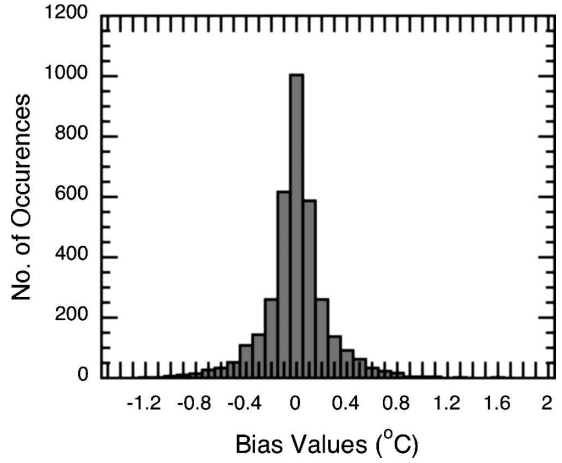

FIG. 6. Histogram for all bias values derived from subtracting the satellite-derived dSST from the observed buoy value.

(0.1 m s^{-1}) an error of 100 W m^{-2} in the maximum SWR can create a difference of 0.4°C in the dSST value and this difference is equal to our average dSST value observed in the comparison dataset.

A possible cause of bias is the fact that the satellite is averaging the solar radiation over 3 h, while the buoy measures the SWR every 2 min (here smoothed by an 18-min running mean). To test this, maximum SWR values for each day were found from the buoy sites using the averaging times used by the satellite data (00Z, 03Z, 06Z, 09Z, 12Z, 15Z, 18Z, and 21Z; Z ≡ UTC). This reduced the overall bias in the peak SWR comparisons to 36.9 W m^{-2} (satellite higher). Therefore the bias produced from using 3-hourly SWR data from the satellite can be reduced by having a much higher resolution of SWR analysis; alternatively, a fit to the solar elevation curve could be used to infer the peak solar radiation. Future work will continue to address this issue. The daily averaged in situ and satellite-measured wind values have much higher correlations than seen from the maximum SWR measurements, with values ranging from 0.64 to 0.93. The overall bias for the wind comparisons is −0.34 with a correlation of 0.84. The dSST values are less sensitive to this bias.

To estimate the random error associated with the variance computed from the solar and wind comparisons, different values of wind speed and maximum SWR values were substituted into a random error equation derived from the Webster et al. (1996) dSST parameterization [Eq. (2)]:

$$\sigma_{SST} = \left\{ [a + d \ln(U^2)]^2 \sigma_{\text{sol}}^2 + \left(\frac{c + d(\text{PS})}{U} + e \right)^2 \sigma_{\text{wnd}}^2 \right\}^{1/2}. \quad (2)$$

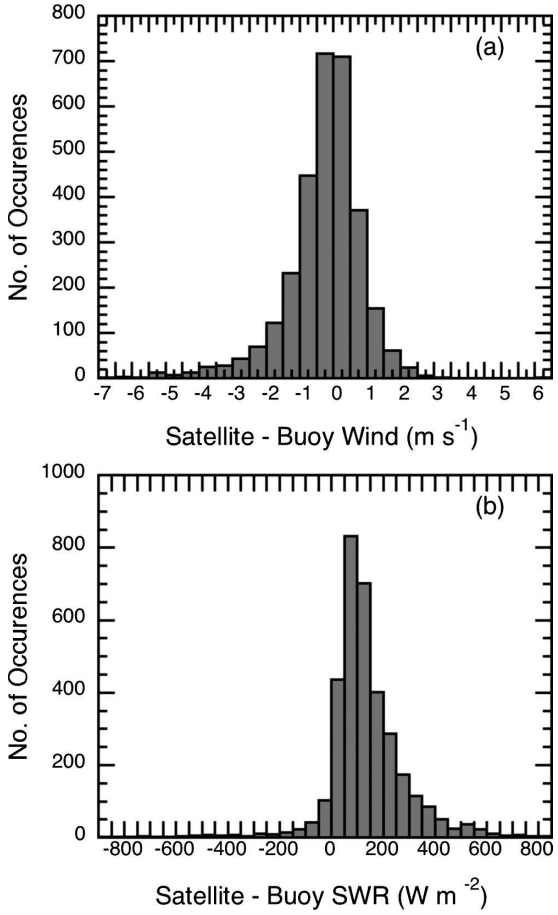

FIG. 7. Histogram for all bias values derived from subtracting the (a) satellite-derived SWR and (b) wind speed from the observed buoy value.

Here σ_{dSST} measures how the standard deviation of dSST will change with variances σ_{sol}^2 (maximum SWR variance) and σ_{wnd}^2 (daily averaged wind speed variance) calculated from the comparison dataset. For this comparison study $\sigma_{\text{sol}}^2 = (151.83)^2$ and $\sigma_{\text{wnd}}^2 = (1.15)^2$; σ_{dSST} calculated from different values of PS and U is shown in Fig. 8. Generally, as U increases (decreases) and PS decreases (increases), the standard deviation becomes less (more). The standard deviation values assume that for a given wind speed there is an equal distribution of maximum SWR observations between 0 and 1000 W m^{-2}. Measurements from these comparisons show that average peak SWR values are roughly 900 W m^{-2} and average wind speed values are roughly 6 m s^{-1}, which according to the chart would give a standard deviation in dSST of 0.20°C. Again, changes in the resolution of SWR or other techniques to improve the SWR peak radiation calculation could substantially reduce this error. These error characteristics will be high-

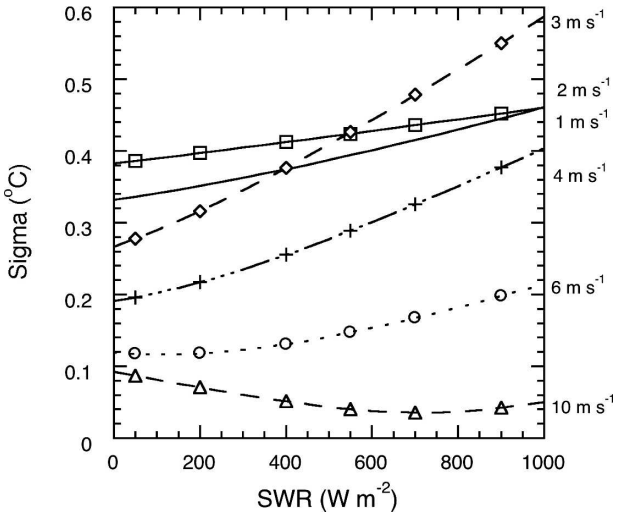

FIG. 8. Theoretical values of standard deviation in dSST measurements with different values of average wind speed and peak SWR.

lighted when they affect results in the following sections.

3. Average diurnal warming values

An average of the dSST data field over the entire five years of the dataset clearly highlights regions with substantial differences from the mean (Fig. 9, values of average peak shortwave radiation and daily averaged wind speed are also shown). The northern Indian Ocean, the western equatorial Pacific, the equatorial eastern Pacific, and several coastal regions including those off of Guinea, western Central America, and northwest Australia all show values above the mean, with values near 1.0°C evident in some localized regions.

Convection along the average placement of the ITCZ (5°N) causes lower values of peak SWR. These lower values of peak SWR along the ITCZ create smaller average dSST values. However, most variations are best explained by the wind speed variability across the basins. This is due to the fact that, throughout most of the tropical regions, peak shortwave radiations fall within a window of 200 W m^{-2}. Wind speeds however average between 3 and 9 m s^{-1}; this variability accounts for a greater portion of the variability in diurnal warming than the 200 W m^{-2} changes in solar radiation. The average wind speeds were around 3–4 m s^{-1} in areas where high average dSST values of 0.7°C were found, while wind speeds greater than 8 m s^{-1} are associated with weak diurnal warming of less than 0.2°C (i.e., south Indian Ocean and tropical north-central Pacific Ocean). Along the Pacific coast of Central America there are large wind speed differences due to gaps in the mountain ranges in that area. Southeasterly winds are funneled through the Chivela Pass in the Sierra Madres and the lake district of Nicaragua, creating very high wind speeds on the Pacific coast side. Where the mountain ranges exist, their high topography acts as a wall to the southeasterly winds and therefore decreases the wind speed in these Pacific coastal regions. These dramatic changes in wind speed have an impact on the dSST, where in regions of gap flow there is on average lower dSST values observed compared to dSST values in regions where mountain ranges are located.

Seasonal extremes in diurnal warming are shown in the 5-yr averages for January and July (Fig. 10). The influence of seasonal variability in SWR from north to south is clear for the Pacific and Atlantic regions. There is a seasonal variability in diurnal warming in the Indian Ocean as well (from highs of 0.6°C to lows of less than 0.2°C), but it is not dependent on the seasonal variability of SWR. During January the monthly averaged wind speeds are generally between 4 and 7 m s^{-1} (Fig. 10) with average peak SWR values greater than 700 W m^{-2}. However, the summer monsoon causes increased surface wind speeds (greater than 9 m s^{-1}) and decreased SWR values (around 500 to 700 W m^{-2}) due to tropical convection. Both of these factors influence the dSST by decreasing its amplitude.

These seasonal differences are affected by year-to-year variability, particularly in the eastern Pacific and Indian Oceans, as can be seen in Fig. 11. The cold tongue region in the eastern Pacific experiences average diurnal warming events in 1998 of over 1.0°C greater than in 1997, with equivalent variability seen off the west coast of Sumatra with the warming occurring in 1997 as compared to 1998. Changes in the Pacific are related to the 1997/98 El Niño and following La Niña; the Indian Ocean was also quite anomalous during this time, but possibly due to local coupled ocean–land–atmosphere interactions (Webster et al. 1999). In the Pacific Ocean, late 1997 had increased SSTs in the cold tongue region, but reduced diurnal warming, with the opposite being true in 1998 (further discussions of these changes can be found in Clayson and Weitlich 2005). Similarly, in the Indian Ocean, off of Sumatra there is an anomalously cool SST field in the east in late 1997, but significantly enhanced solar radiation that results in enhanced diurnal warming. The opposite again is true in 1998, with mean diurnal warming values being reduced by as much as 1.5°C due to stronger winds, consistent with the dipole model of the Indian Ocean dipole (IOD) in 1998 (Saji et al. 1999). In both locations,

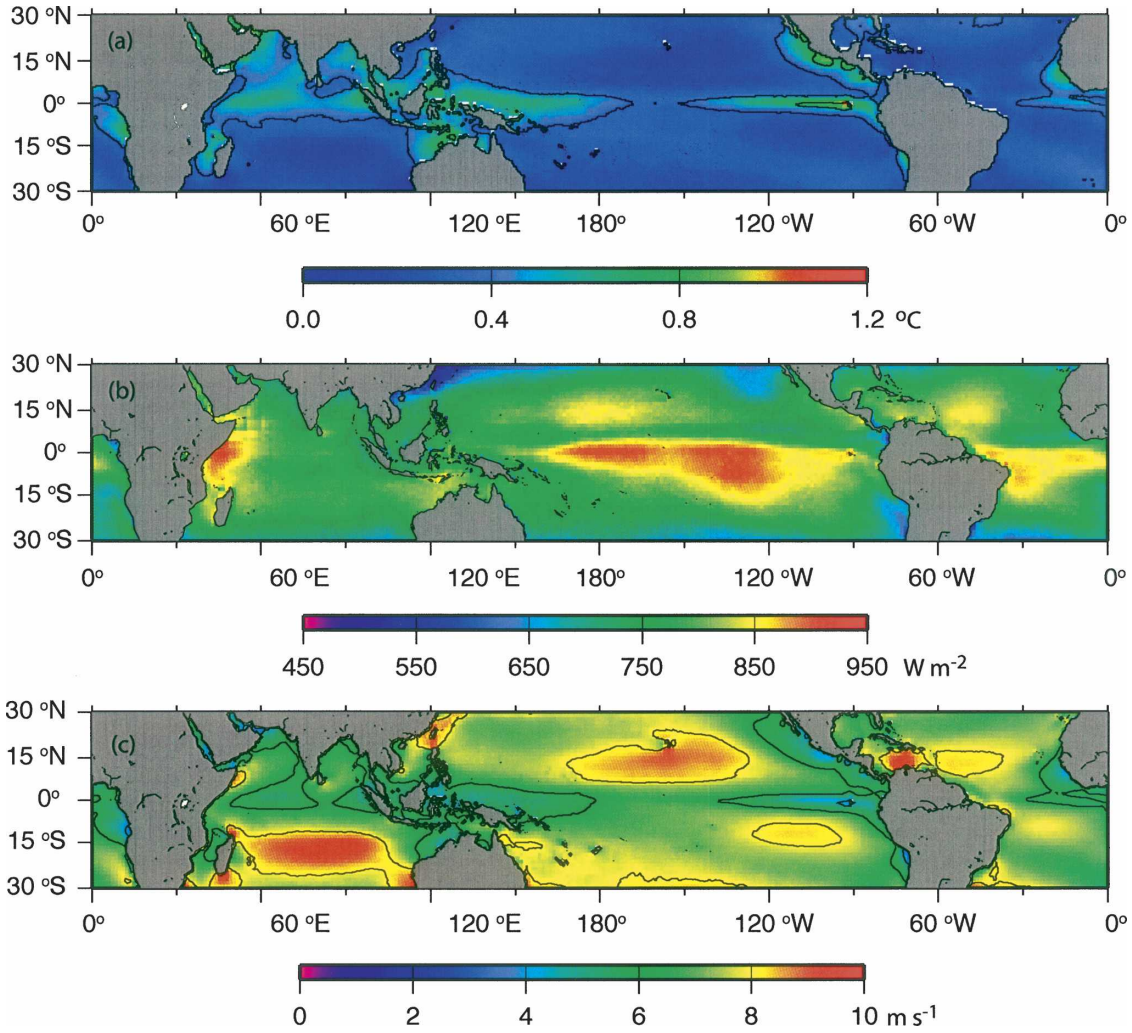

FIG. 9. (a) The dSST values averaged from 1 Jan 1996 through 31 Dec 2000; (b) average wind speed values; and (c) average peak SWR values.

differences between the years are caused both by changes in wind speed and SWR. The key factor is that during one of these periods the wind speeds became very light (less than 3 m s^{-1} on average). Since the response of diurnal warming is nonlinear, other changes in wind speed in the Tropics that are comparable to these but at the higher end of the wind speed regime do not show such substantial differences.

4. Interannual variability

To further examine patterns of large-scale variability in dSST, an EOF analysis of the data was performed in each tropical ocean basin (Atlantic, Indian, and Pacific). The variances accounted for by the first three modes in each ocean basin are shown in Table 3. The results shown are those for an analysis of 5-day-averaged data. An examination of EOF analyses for the daily values shows nearly identical spatial and mean temporal variability but with significantly higher small-scale variability and correspondingly less percentage of the variance explained. Since the focus of this study is on the large-scale variability, an examination of these smaller temporal fluctuations in the principal component time series will be deferred. Overland and Preisendorfer (1982) determined a method for evaluating whether, given a specific sample size and time series length, the variances calculated were significantly different from noise (for this number of samples in space and time, the variance due to noise would be roughly 1.0). According to this "Rule N," each of the modes shown in this paper is significantly different from noise.

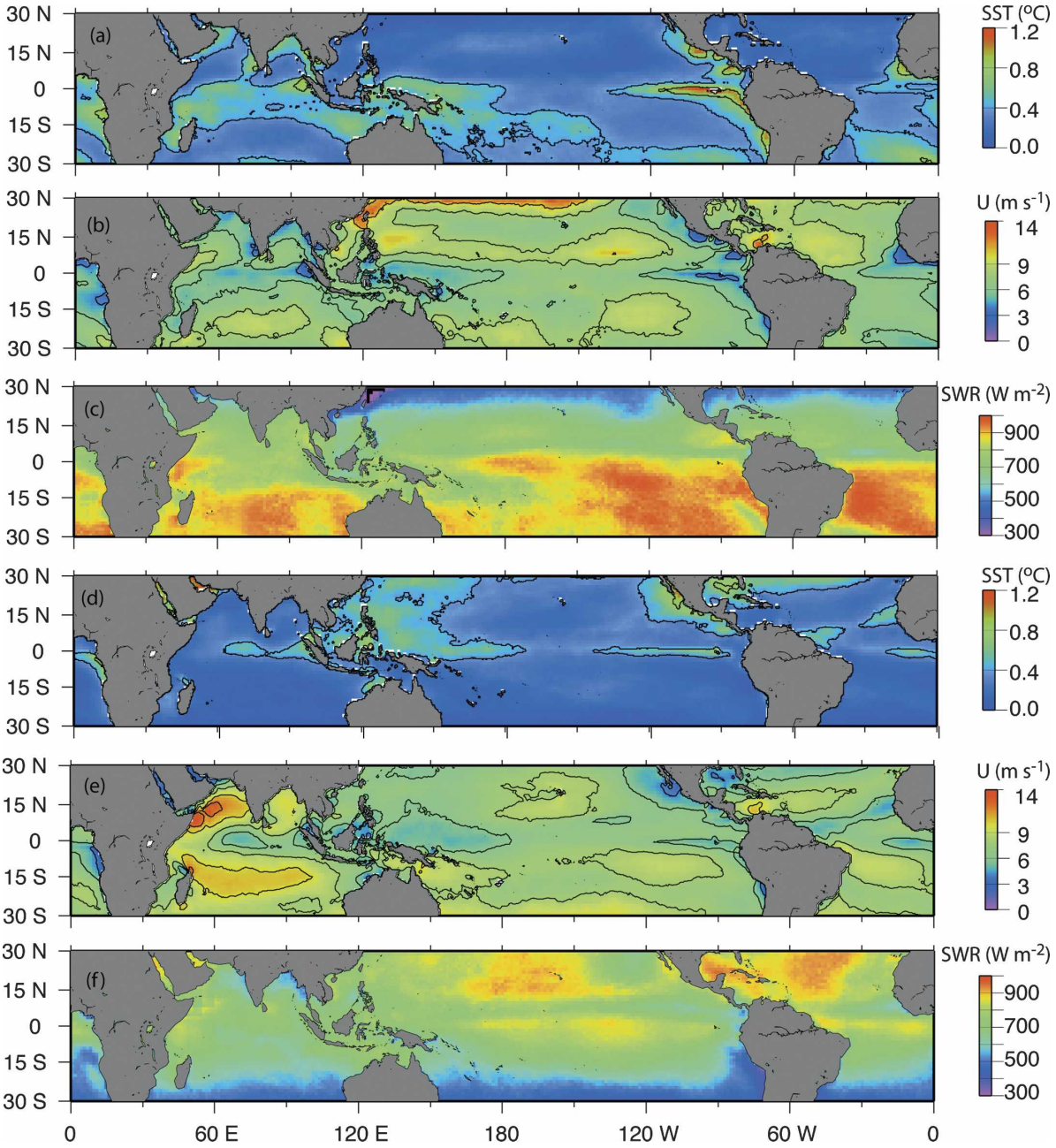

FIG. 10. Average dSST values in the Tropics for (a) January and (d) July during the entire period studied (1996–2000). Average wind speed values for (b) January and (e) July and average SWR values for (c) January and (f) July are also shown. Colors and contours are consistent between the January and July averages, with contours of 0.4°C in dSST and every 2 m s^{-1} in wind speed.

Using North's "Rule of Thumb" (North et al. 1982), the sampling error for each of the variances shown is smaller than the sampling error of the nearest eigenvectors, meaning that each of the EOFs shown in this paper is significant within a 95% confidence interval.

From Table 3 it is apparent that the Indian Ocean has the most cohesive patterns of variances, with the Pacific Ocean the least. This is perhaps to be expected given the significantly larger area of the Pacific and the larger number of unrelated synoptic events encompassed by this basin. The first three mode spatial patterns and their corresponding principal component time series are shown respectively for the Atlantic (Fig. 12), the Indian (Fig. 13), and the Pacific (Fig. 14) Oceans. There

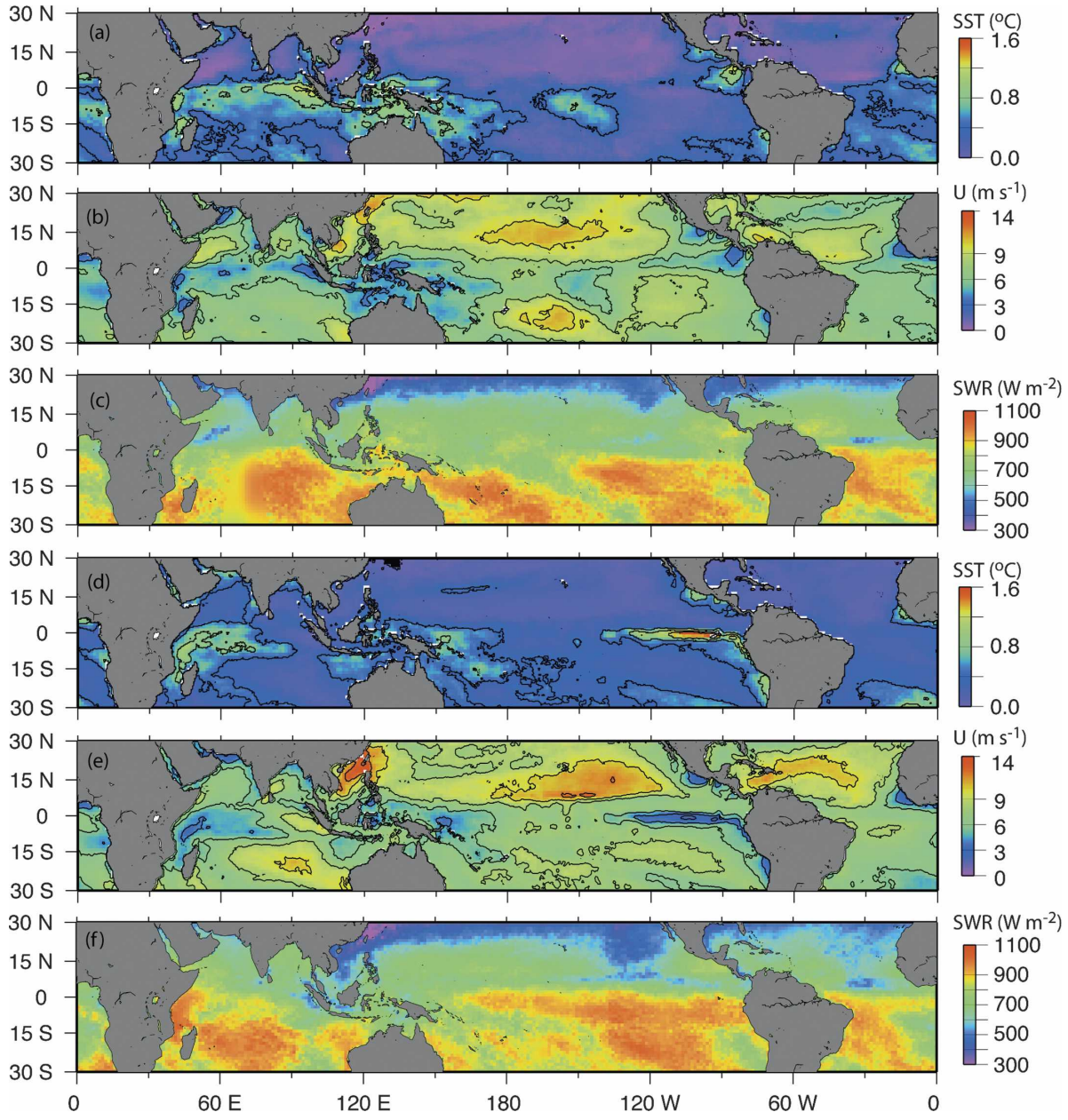

FIG. 11. Average dSST values in the Tropics for (a) December 1997 and (d) December 1998. Average wind speed values for (b) December 1997 and (e) December 1998 and average SWR values for (c) December 1997 and (f) December 1998 are also shown. Colors and contours are consistent between the January and July averages, with contours of 0.4°C in dSST and every 2 m s^{-1} in wind speed.

are a number of similar characteristics between the three basins, and these as well as their differences are discussed below.

a. Hemispheric seasonal variability

For all ocean basins, mode 1 shows the seasonal variability of dSST that was illustrated in Fig. 10. In the tropical Atlantic and Pacific Oceans there are mostly negative weights that dominate the NH and positive weights that dominate the SH. The time coefficients are generally positive from October to March and negative from April to September, indicating above-mean dSST values in the SH and below-mean values in the NH for boreal winter, with the opposite being true for boreal summer. This seasonal variability is due to the annual cycle of solar radiation as discussed previously. This cycle is fairly constant throughout the observational period (as can be demonstrated by an EOF analysis of the

TABLE 3. Percent of variance explained in each of the first three modes of the EOF analysis using 5-day-averaged dSST values.

Tropical ocean basin	Mode 1, mode 2, mode 3; cumulative
Atlantic	22.3%, 8.8%, 5.9%; 37.0%
Indian	26.2%, 10.9%, 5.8%; 42.9%
Pacific	15.1%, 8.2%, 5.1%; 28.4%

shortwave radiation, such as that for mode 1 in the Atlantic as shown in Fig. 15) and, therefore, there is little interannual variability between the different years for this mode.

However, as also mentioned previously, the Indian Ocean does not follow this same trend. The first mode for the Indian Ocean displays mostly positive weights with weights greater than 0.5 dominating from 15°S northward. Therefore, both hemispheres follow the same trend of above-mean or below-mean values. Higher amplitude positive time coefficients (above 0.1°C) occur around March and April, corresponding to diurnal warming values greater than 0.4°C above the mean in the Arabian Sea, the Bay of Bengal, and directly east of Somalia. Equal magnitude negative weights transpiring from May to August correspond to below-average values of around 0.4°C for these areas. From October to December the time coefficients are very small so that dSST values are close to mean values for the entire basin during this time. This variability is due to the summer monsoon, as the monsoon trough lies over northern India during the months where nega-

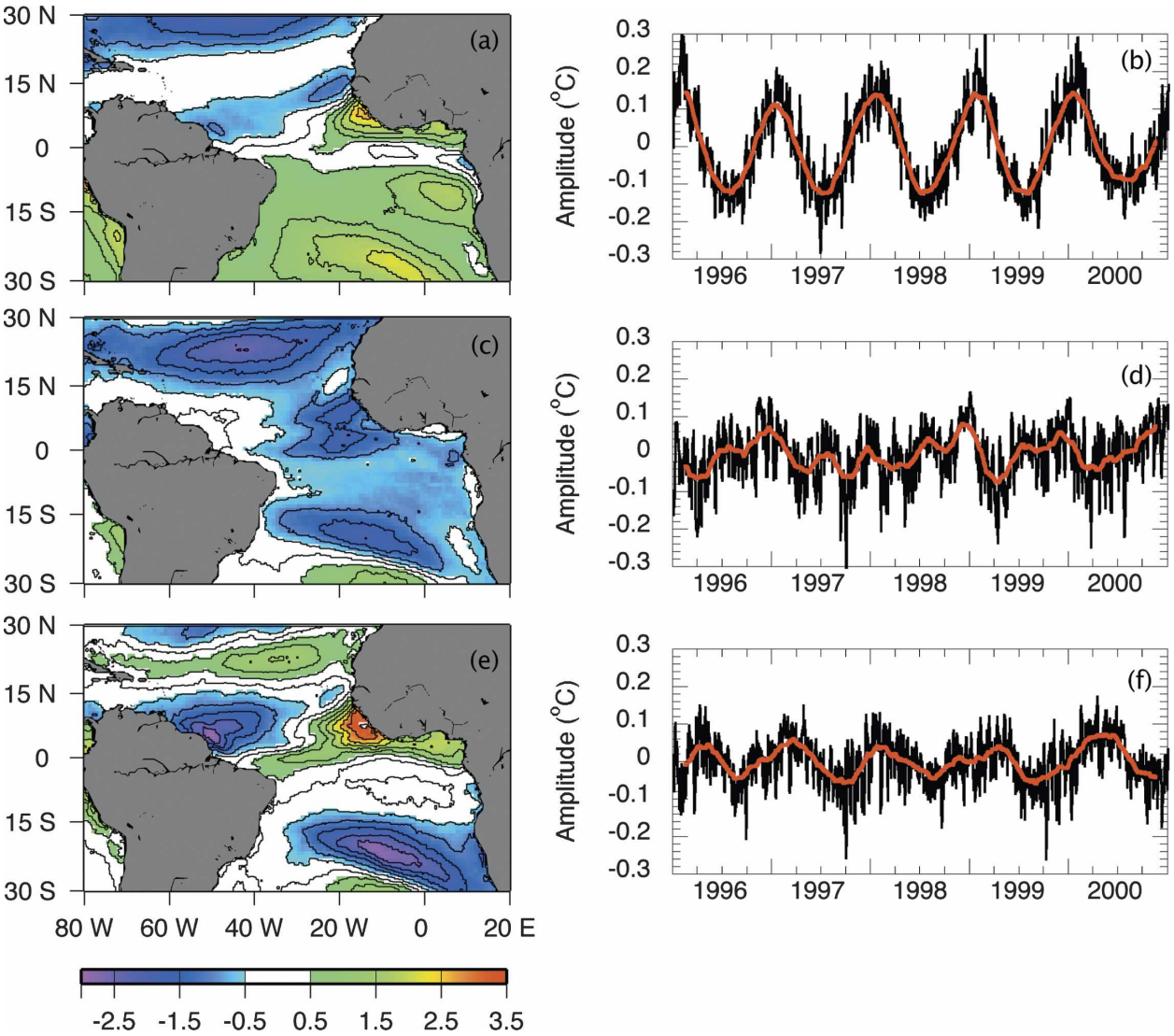

FIG. 12. The dSST EOF spatial patterns and principal component time series for (a), (b) mode 1, (c), (d) mode 2, and (e), (f) mode 3 in the tropical Atlantic Ocean. Heavy red line indicates 3-month running average.

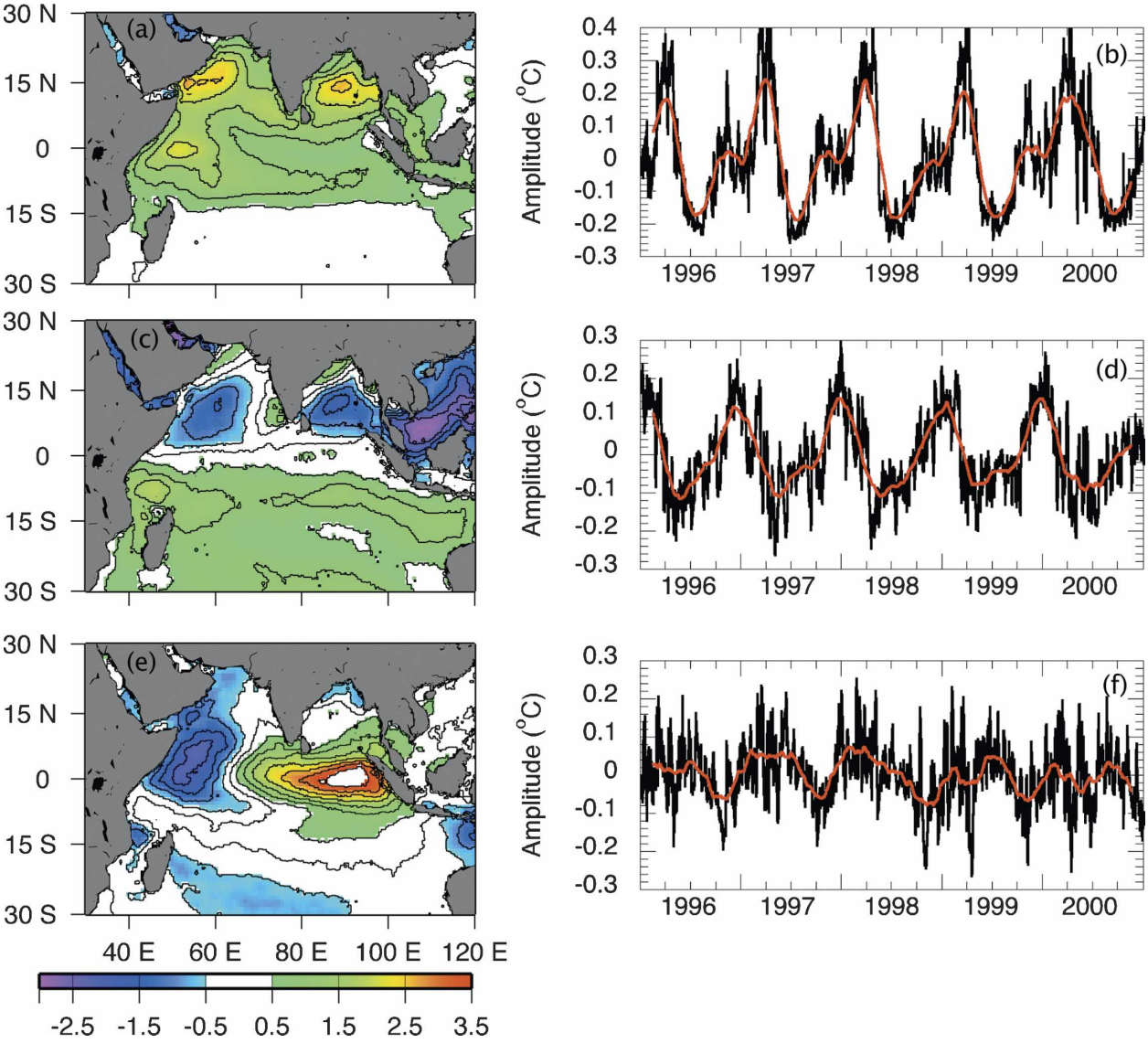

FIG. 13. As in Fig. 12 but for the tropical Indian Ocean.

tive time coefficients occur and brings with it deep convection and rainfall over most of the ocean basin. Also, during these months the low-level cross-equatorial jet that resides around 1 km (and influences the surface winds) is at its strongest (e.g., Findlater 1971). The monsoonal flow during boreal summer is much stronger and more concentrated than during winter (e.g., Webster et al. 1998), causing a decrease in diurnal warming in the summer compared to the winter. This mode also shows little yearly difference.

The secondmost variance-explaining mode in the Indian Ocean is due to the seasonal cycle of SWR. Negative weights occur mostly in the NH and positive weights are widespread in the SH. The principal component time series of mode 2 also shows an annual cycle. The annual cycle in this mode tends to be shifted about a month earlier in its pattern compared to the cycles viewed in mode 1 for the Atlantic and Pacific with negative time coefficients dominating March to August and positive time coefficients prevailing from April to December, due to increased cloudiness during March–August and decreased cloudiness thereafter.

b. East–west dipole

In each basin there also exists an east–west ocean dipole of strong negative weights and positive weights. In the tropical Pacific it occurs in mode 2 and in the Atlantic and Indian Oceans it occurs in mode 3. For the Atlantic and Indian Oceans positive weights up to 3.5 can be found in the eastern part of the ocean, with

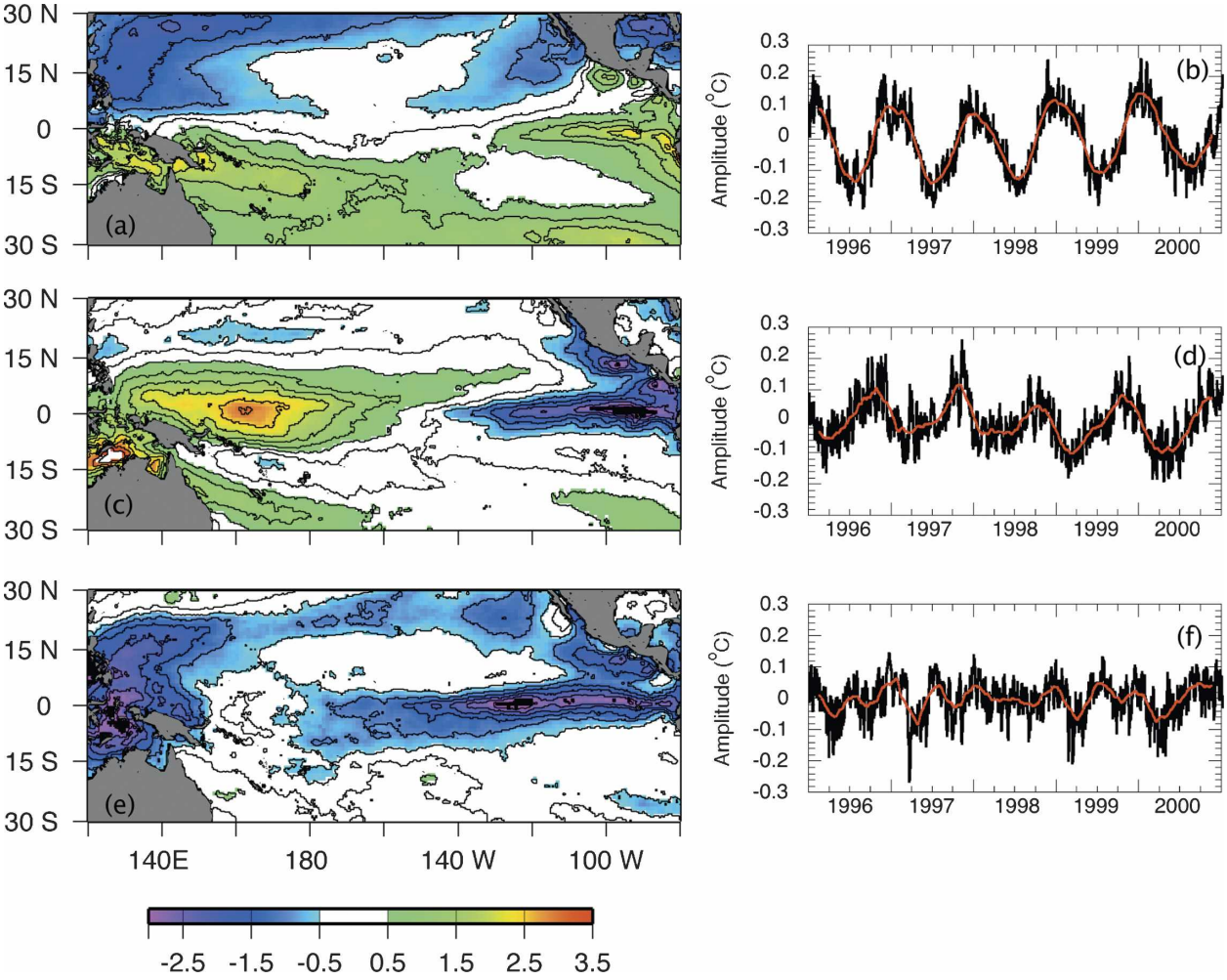

FIG. 14. As in Fig. 12 but for the tropical Pacific Ocean.

lower magnitude negative weights (−2 to −2.5) in the western region. Thus, higher variability is found in the eastern areas for both of these ocean basins. Also, the dipole in the Indian Ocean is generally located along the equator, but in the Atlantic it is shifted northward. In the Pacific, negative weights up to −3 are found in the eastern equatorial zone and positive weights of equal magnitude are found in the western equatorial region.

The principal-component time series for each of these modes show a general annual cycle with some changes year to year. For mode 3 in the Atlantic Ocean there is a general pattern of positive time coefficients from October to May (above-average dSST in the east and below-average dSST in the west) and negative time coefficients from June through September (below-average dSST in the east and above-average dSST in the west). This dipole effect in the Atlantic is mainly due to the migration of the Atlantic ITCZ. The ITCZ in the Atlantic during boreal winter and spring resides close to the equator in the western Atlantic Ocean, bringing with it convective cloud cover and precipitation in this region (Grodsky and Carton 2003). This would lead to smaller peak SWR values during the day in the eastern Atlantic compared to the western Atlantic and therefore smaller dSST values in the east and larger dSST values in the west. During boreal summer, the ITCZ shifts north and produces greater cloudiness and rainfall in the eastern Atlantic around 8°N (Chiang et al. 2002). Also during this time intense heating of the Sahara creates a meridional gradient in pressure with a heat low over the Sahara and a high pressure system to the south over the Gulf of Guinea producing a shallow westerly monsoon flow in the eastern Atlantic (Carlson 1969). Maximum wind speeds from this westerly jet can exceed 7 m s^{-1} (Grodsky et al. 2003). The combination of stronger monsoon flow and decreased SWR values over the eastern Atlantic causes smaller dSST values in

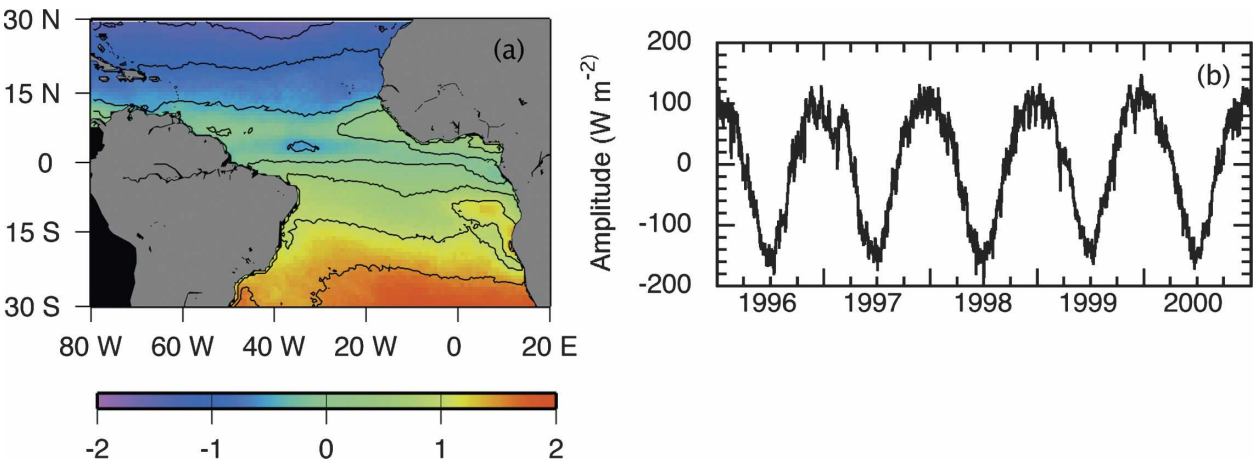

FIG. 15. Peak shortwave radiation (a) spatial pattern and (b) principal component time series for mode 1 in the tropical Atlantic Ocean. This mode describes 27.7% of the SWR variance.

the eastern Atlantic than those found in the western Atlantic.

In the Indian Ocean, for mode 3, and the Pacific Ocean, for mode 2, positive coefficients dominate in the first half of the year and negative coefficients occur around the latter half of the year. This shows that dSST values around the first (last) six months are above (below) average in the east and below (above) average in the west. These seasonal variable patterns of dSST display the same variability of longer interannual variations in SSTs found in each of these basins, namely the newly discovered IOD in the tropical Indian Ocean and ENSO in the tropical Pacific.

The IOD is an anomaly with a positive phase with cooler than average SSTs in the eastern Indian Ocean off the west coast of Sumatra and warmer than average SSTs in the western Indian Ocean with associated convection and precipitation (Saji et al. 1999). The negative phase of the IOD reverses the SST gradients, and therefore greater convection and precipitation forms over the warmer waters of the eastern Indian Ocean. The IOD tends to have a biennial tendency tied to monsoon–ocean feedback (Wang et al. 2003). A strong positive IOD event occurred during 1997; however during this particular IOD event little effect was seen on the seasonal variability of the dSST dipole.

This is not the case in the Pacific where the overlying ENSO pattern does show some influence on mode 2 for this region. Examination of the time series for this mode shows that comparing the December 1997–March 1998 (El Niño) period to the December 1998–March 1999 (La Niña) period that the negative coefficients during this period have a higher magnitude in the La Niña period. This is also true for the La Niña event from December 1999–March 2000. This means that during the La Niña years greater above-average dSST values are observed in the eastern Pacific and greater below-average dSST values occurs in the western Pacific compared to the El Niño period. This opposite trend in dSST compared to SSTs for ENSO was exactly what was observed in the average files examined earlier and was due to variations in the average peak SWR and daily averaged wind speeds, and agrees with the analysis of Cronin and Kessler (2002)who analyzed buoy data from the eastern Pacific. Implications of this pattern and possible effects on entrainment cooling are discussed more fully in Clayson and Weitlich (2005).

5. Summary and discussion

Comparisons of diurnal range measurements from the buoy and satellite-derived values showed an overall correlation of 0.74 and a small average bias of −0.002°C. The main differences between the datasets were shown to be due to an underestimation of peak SWR by the satellite, caused by the 3-hourly sampling interval. Ongoing work is dedicated to using appropriate interpolation techniques to estimate the peak solar radiation from the 3-hourly data. These statistics suggest that the means and variability of the diurnal warming discussed within the paper are realistic. However, it is difficult to state with certainty the absolute error characteristics of the satellite-derived field as the buoys are measuring the SST, not from radiometers measuring the skin, but at depth within the ocean. This could affect the diurnal variability of the buoys such that calculating diurnal warming from these values could be underestimating the diurnal variation of the skin temperature due to the fact that, at the highest solar radiation and minimum wind speeds, the warming may be

concentrated in a layer above the depth of the buoy measurement (e.g., Fairall et al. 1996). Comparisons with radiometer data would be the most accurate means of comparison, but these measurements are very few in number. In addition, the parameterization used in this analysis was based on one turbidity profile through the upper ocean; changing between the various types (such as Jerlov Type I to Type III) could, under very light winds and high solar insolation, change the dSST value by as much as 0.3°C (or roughly 10%) based on our model simulations. This source of uncertainty, and how to implement this variability across the Tropics, will be the focus of future research.

Five-year-averaged dSST values in the Tropics showed diurnal warming values up to 1°C. The variability of the mean across the basins was most influenced by the wind speed variations from location to location, as the differences in peak SWR across the basins in general were small enough to preclude a significant variation in diurnal warming. Monthly averaged variations between years and seasons could reach values of 2°C. The most evident of the yearly changes are found between 1997 and 1998 in the regions of the cold tongue in the eastern Pacific, the equatorial central Pacific, and in the eastern Indian Ocean.

These yearly changes are most evident in regions of lower wind speed, where small changes in wind speed and/or SWR more strongly affect the maximum diurnal warming. This effect is summarized in Fig. 16, which shows the change in dSST at each location between December 1997 and December 1998 with respect to changes in wind speed and shortwave radiation. The minimum wind speed of the two time periods is shown by the color of the plotted points. The observed changes in solar radiation, while substantial, do not cause a difference in the diurnal warming in those regions where the wind speeds are large. This is true as well for even large differences in mean wind speed, when the minimum wind speed is still substantially larger than a few m s^{-1}. Thus those regions that are more prone to smaller wind speeds are more likely to show seasonal or interannual variability in diurnal warming. It should be noted that, since these are comparisons between December values, the changes in solar radiation are due to changes in cloud properties rather than simply solar elevation angles.

The influence of seasonal variability on the diurnal warming can be seen in the most dominant EOF mode. For the Atlantic and Pacific during boreal summer (winter), above- (below-) average dSST values occur in the NH and below- (above-) average dSST values are found in the SH. This seasonal cycle is dominated by the SWR yearly cycle. The seasonal variability in the

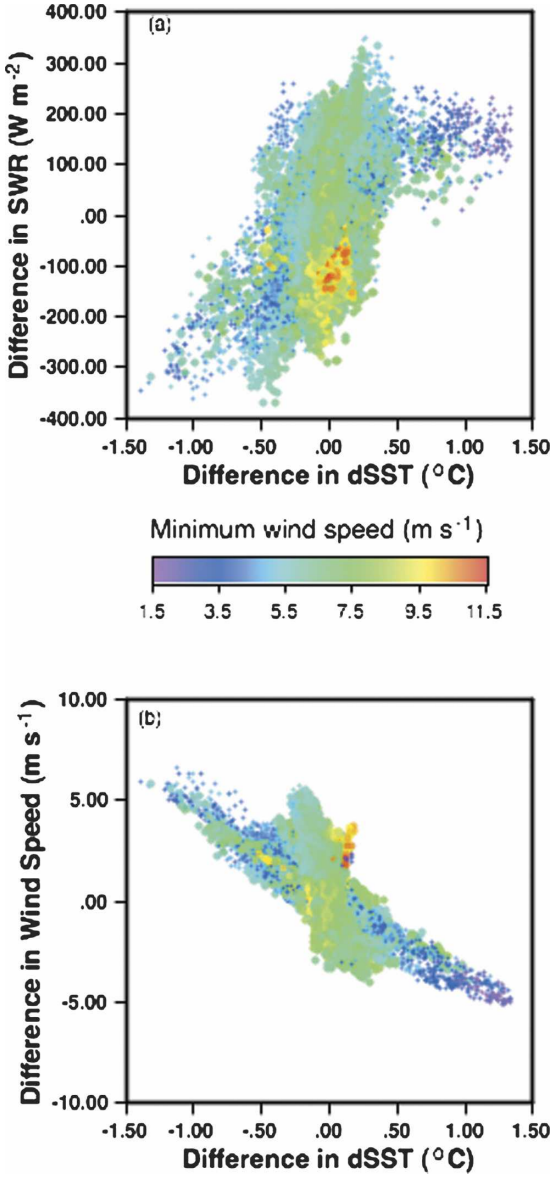

FIG. 16. Point to point changes in dSST between December 1997 and December 1998, as compared to the changes in (a) SWR and (b) wind speed. The color scale is based on the minimum wind speed at that point between the December 1997 and December 1998 means.

Indian Ocean that explains the largest percent of the variance is however due to monsoonal flow. Increased convection during the summer monsoon in the Northern Hemisphere and strong winds from the low-level cross-equatorial jet during the boreal summer on average increase the diurnal warming by more than 0.5°C, with similar cooling amounts occurring during the other months of the year. Seasonal variability due to the annual solar declination angle cycle is also important in mode 2 in the Indian Ocean; the variance explained by

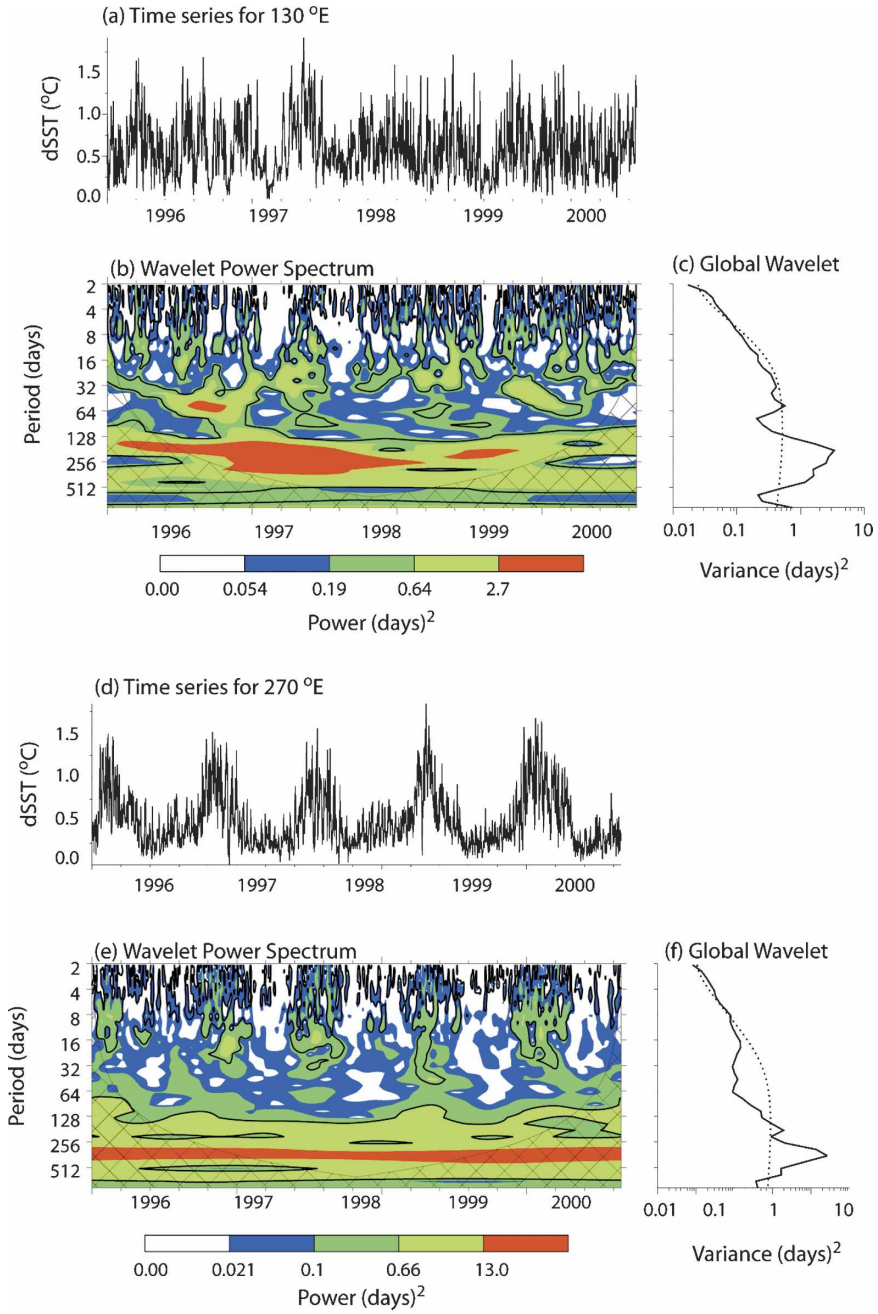

FIG. 17. (a) Time series of dSST values for 1996–2000 at 0°, 130°E; (b) wavelet power spectrum from the time series in (a); and (c) variance of the global wavelet for the time series in (a). Dark lines in (b) indicate when values are significant; cross-hatching indicates when analysis is not appropriate due to edge effects. Dashed line in (c) shows significance level; values above this (to the right) are significant. (d)–(f) As in (a)–(c) but for 0°, 270°E.

seasonal variability in this basin is over one-third of the total variance, which is much greater than that explained by seasonal variability in either the Atlantic or Pacific basins. In general, the first-mode seasonal variability shows essentially no year-to-year variability in the mean. The Atlantic and Pacific time series are essentially sinusoidal, while the Indian Ocean (because of its dependence on the monsoon and not seasonal solar variability) has a several-month period at the end of the year with zero temporal coefficients.

East–west dipole weight structures appear in the spatial patterns for mode 2 in the Pacific and mode 3 for

the Atlantic and Indian Oceans. All patterns in these modes have some seasonally varying characteristics. The Atlantic dSST dipole seasonal variability is due to changes in the West African monsoon and the seasonal placement of the ITCZ. The dipole in the Indian and Pacific Oceans resembles the biennial patterns of the IOD and ENSO, respectively, with above (below) average dSST values for the east (west) ocean basin during the first half of the year and below (above) average dSST values for the west (east) part of the basin. The annual cycle of the dipole pattern in mode 2 for the Pacific showed interannual differences confirming the results found from the average dSST files for each year: mainly an increase in above-average (higher) diurnal warming for the east Pacific during the La Niña periods of 1998 and 1999 compared to the El Niño of 1997.

As can be seen in the EOF time series and in Fig. 17, there is variability occurring within the diurnal warming fields on much smaller time scales than those focused on here. In all of the basins, the east–west dipole time series shows variability about the mean of more than 100% of the mean; in some cases values are 3 times the mean value. Clear dependence of the diurnal warming on intraseasonal variability is evident here and should be expected given the dependence of cloud variability and winds in the Tropics on intraseasonal events such as the Madden Julien oscillation, monsoon breaks, 2–3-day convective variability, and other processes. Variability on the shorter time scales can easily be seen by perusal of the wavelet power spectrums in Fig. 17. For both locations, variability is significant in the 2–4-day period, although in the western part of the basin this variability happens fairly consistently throughout the time series (except in mid-1997), while in the eastern part of the basin power at this frequency tends to be significant only in the boreal winter periods. Conversely, variability at periods greater than 4 months, especially seasonal, is apparent throughout the 5-yr time period in the eastern Pacific, while the strength of the variability at these periods is much stronger in 1996 through 1998 in the western Pacific. Significant variability in the 30–90-day time period is especially evident in the western Pacific during late 1996 and 1997, perhaps consistent with MJO variability. These results agree with the analysis of an eastern Pacific buoy by Cronin and Kessler (2002), who found a strong seasonal dependence at this place of diurnal SST (with maximum values during the warm season). Clearly their results are very dependent on the atmospheric and ocean dynamics in the region; characterization of the diurnal warming signal will help in understanding the roles each of these play as well as feedbacks between the diurnal SST and these longer time-scale events.

Acknowledgments. We acknowledge with pleasure the support by the NASA Physical Oceanography program under Grant 1218935. SSM/I data (www.remss.com) are produced by Remote Sensing Systems and sponsored by the NASA Earth Science REASoN DISCOVER Project. The buoy data were provided by the TAO Project Office. We are grateful to Yuanchong Zhang for the special processing of the ISCCP-FDX data.

REFERENCES

Bourassa, M. A., D. G. Vincent, and W. L. Wood, 1999: A flux parameterization including the effects of capillary waves and sea state. *J. Atmos. Sci.,* **56,** 1123–1139.

——, D. M. Legler, J. J. O'Brien, and S. R. Smith, 2003: SeaWinds validation with research vessels. *J. Geophys. Res.,* **108,** 3019, doi:10.1029/2001JC001028.

Carlson, T. N., 1969: Synoptic histories of three African disturbances that developed into Altantic hurricanes. *Mon. Wea. Rev.,* **97,** 256–276.

Chang, P., L. Ji, and H. Li, 1997: A decadal climate variation in the tropical Atlantic Ocean from thermodynamic air-sea interactions. *Nature,* **385,** 516–518.

Chiang, J. C. H., Y. Kushnir, and A. Giannini, 2002: Deconstructing Atlantic Intertropical Convergence Zone variability: Influence of the local cross-equatorial sea surface temperature gradient and remote forcing from the eastern equatorial Pacific. *J. Geophys. Res.,* **107,** 4004–4022.

Clayson, C. A., and J. A. Curry, 1996: Determination of surface turbulent fluxes for TOGA COARE: Comparison of satellite retrievals and in situ measurements. *J. Geophys. Res.,* **101,** 28 503–28 513.

——, and A. Chen, 2002: Sensitivity of a coupled single-column model in the Tropics to treatment of the interfacial parameterizations. *J. Climate,* **15,** 1805–1831.

——, and D. Weitlich, 2005: Interannual variability of tropical Pacific diurnal sea surface temperature warming and nighttime cooling. *Geophys. Res. Lett.,* **32,** L21604, doi:10.1029/2005GL023786.

Cronin, M. F., and W. S. Kessler, 2002: Seasonal and interannual modulation of mixed layer variability at 0°, 110°W. *Deep-Sea Res. I,* **49,** 1–17.

Deschamps, P. Y., and R. Frouin, 1984: Large diurnal heating of the sea surface observed by the HCMR experiment. *J. Phys. Oceanogr.,* **14,** 177–184.

Fairall, C. W., E. F. Bradley, J. S. Godfrey, G. A. Wick, J. B. Edson, and G. S. Young, 1996: Cool-skin and warm-layer effects on sea surface temperature. *J. Geophys. Res.,* **101,** 1295–1308.

Findlater, J., 1971: Mean monthly airflow at low levels over the western Indian Ocean. *Geophys. Mem.,* **16,** 1–53.

Gentemann, C. L., C. J. Donlon, A. Stuart-Menteth, and F. J. Wentz, 2003: Diurnal signals in satellite sea surface temperature measurements. *Geophys. Res. Lett.,* **30,** 1140, doi:10.1029/2002GL016291.

Grodsky, S. A., and J. A. Carton, 2003: Intertropical convergence zone in the South Atlantic and the equatorial cold tongue. *J. Climate,* **16,** 723–733.

——, ——, and S. Nigam, 2003: Near surface westerly wind jet in the Atlantic ITCZ. *Geophys. Res. Lett.,* **30,** 2009, doi:10.1029/2003GL017867.

Halpern, D., and R. K. Reed, 1976: Heat budget of the upper ocean under light winds. *J. Phys. Oceanogr.,* **6,** 972–975.

Huang, B., and J. Shukla, 1997: Characteristics of the interannual and decadal variability in a general circulation model of the tropical Atlantic Ocean. *J. Phys. Oceanogr.,* **27,** 1693–1712.

Imaoka, K., and R. W. Spencer, 2000: Diurnal variation of precipitation over the tropical oceans observed by TRMM/TMI combined with SSM/I. *J. Climate,* **13,** 4149–4158.

Kawai, Y., and H. Kawamura, 2002: Evaluation of the diurnal warming of sea surface temperature using satellite-derived marine meteorological data. *J. Oceanogr.,* **58,** 805–814.

Mapes, B. E., and R. A. Houze Jr., 1995: Diabatic divergence profiles in western Pacific mesoscale convective systems. *J. Atmos. Sci.,* **52,** 1807–1828.

McPhaden, M. J., and Coauthors, 1998: The Tropical Ocean-Global Atmosphere observing system: A decade of progress. *J. Geophys. Res.,* **103,** 14 169–14 240.

Mears, C. A., D. K. Smith, and F. J. Wentz, 2001: Comparison of Special Sensor Microwave Imager and buoy-measured wind speeds from 1987 to 1997. *J. Geophys. Res.,* **106,** 11 719–11 729.

North, G. R., T. L. Bell, R. F. Cahalan, and F. J. Moeng, 1982: Sampling errors in the estimation of empirical orthogonal functions. *Mon. Wea. Rev.,* **110,** 699–706.

Overland, J. E., and R. W. Preisendorfer, 1982: A significance test for principal components applied to a cyclone climatology. *Mon. Wea. Rev.,* **110,** 1–4.

Payne, R. E., and Coauthors, 2002: A comparison of buoy meteorological systems. WHOI Tech. Rep. WHOI-2002-10, Woods Hole Oceanographic Institution, 67 pp.

Perigaud, C., D. Neelin, and J. McCreary, 2003: Role of the Indian Ocean SST anomalies in the coupling of the atmosphere and ocean. Preprints, *12th Conf. on Interactions of the Sea and Atmosphere,* Long Beach, CA, Amer. Meteor., Soc., CD-ROM, 6.4.

Price, J. F., R. A. Weller, and R. Pinkel, 1986: Diurnal cycling: Observations and models of the upper ocean response to diurnal heating, cooling, and wind mixing. *J. Geophys. Res.,* **91,** 8411–8427.

Rossow, W. B., and Y.-C. Zhang, 1995: Calculation of surface and top of atmosphere radiative fluxes from physical quantities based on ISCCP data sets. 2. Validation and first results. *J. Phys. Res.,* **100,** 1167–1197.

Saji, N. H., B. N. Goswami, P. N. Vinayachandran, and T. Yamagata, 1999: A dipole mode in the tropical Indian Ocean. *Nature,* **401,** 360–363.

Servain, J., and Coauthors, 1998: A Pilot Research Moored Array in the Tropical Atlantic (PIRATA). *Bull. Amer. Meteor. Soc.,* **85,** 167–172.

Seze, G., and W. B. Rossow, 1991: Effects of satellite data resolution on measuring the space-time variations of surfaces and clouds. *Int. J. Remote Sens.,* **12,** 921–952.

Shinoda, T., 2005: Impact of the diurnal cycle of solar radiation on intraseasonal SST variability in the western equatorial Pacific. *J. Climate,* **18,** 2628–2636.

Solomon, A., and F.-F. Jin, 2005: A study of the impact of off-equatorial warm pool SST anomalies on ENSO cycles. *J. Climate,* **18,** 274–287.

Soloviev, A., and R. Lukas, 1997: Observation of large diurnal warming events in the near-surface layer of the western equatorial warm pool. *Deep-Sea Res.,* **44,** 1055–1076.

Stommel, H., 1969: Observations of the diurnal thermocline. *Deep-Sea Res.,* **16,** 269–284.

Stramma, L., P. Cornillon, R. A. Weller, J. F. Price, and M. G. Briscoe, 1986: Large diurnal sea surface temperature variability: Satellite and in situ measurements. *J. Phys. Oceanogr.,* **16,** 345–358.

Stuart-Menteth, A. C., I. S. Robinson, and P. G. Challenor, 2003: A global study of diurnal warming using satellite-derived sea surface temperature. *J. Geophys. Res.,* **108,** 3155, doi:10.1029/2002JC001534.

Sui, C. H., X. Li, K. M. Lau, and D. Adamec, 1997: Multiscale air–sea interactions during TOGA COARE. *Mon. Wea. Rev.,* **125,** 448–462.

Wang, B., R. Wu, and T. Li, 2003: Atmosphere–warm ocean interaction and its impacts on Asian–Australian monsoon variation. *J. Climate,* **16,** 1195–1211.

Webster, P. J., and R. Lukas, 1992: TOGA COARE: The Coupled Ocean–Atmosphere Response Experiment. *Bull. Amer. Meteor. Soc.,* **73,** 1377–1416.

——, C. A. Clayson, and J. A. Curry, 1996: Clouds, radiation, and the diurnal cycle of sea surface temperature in the tropical western Pacific. *J. Climate,* **9,** 1712–1730.

——, V. O. Magaña, T. N. Palmer, J. Shukla, R. A. Tomas, M. Yanai, and T. Yasunari, 1998: Monsoons: Processes, predictability, and the prospects for prediction. *J. Geophys. Res.,* **103,** 14 451–14 510.

——, A. M. Moore, and R. R. Leben, 1999: Coupled ocean-atmosphere dynamics in the Indian Ocean during 1997–1998. *Nature,* **401,** 356–360.

Wentz, F. J., 1997: A well-calibrated ocean algorithm for special sensor microwave/imager. *J. Geophys. Res.,* **102,** 8703–8718.

Zhang, Y.-C., W. B. Rossow, and A. A. Lacis, 1995: Calculation of surface and top of atmosphere radiative fluxes from physical quantities based on ISCCP data sets. 1. Method and sensitivity to input data uncertainties. *J. Geophys. Res.,* **100,** 1149–1165.

——, ——, ——, V. Oinas, and M. I. Mishchenko, 2004: Calculation of radiative fluxes from the surface to top of atmosphere based on ISCCP and other global data sets: Refinements of the radiative transfer model and the input data. *J. Geophys. Res.,* **109,** D19105, doi:10.1029/2003JD004457.